J Mater Sci: Mater Electron (2017) 28:12670–12682
DOI 10.1007/s10854-017-7092-2

Degradation of methyl orange and removing Pb^{2+} from the water with ZnO–Fe nano photocatalyst

Mohammad Sabet[1] · Samira Saeednia[1] · Mehdi Hatefi-Ardakani[1] · Roya Sheykhisarem[1]

Received: 26 March 2017 / Accepted: 5 May 2017 / Published online: 15 May 2017

Abstract In this work, ZnO–Fe nanostructures with different morphologies were synthesized via a simple hydrothermal method. Different parameters such as surfactant, reaction time and temperature, Fe source value, and Zn source kind were changed to the investigation of each parameter on the product size and morphology. The results obtained from SEM images showed each parameter has a significant effect on the product size and morphology. Also, the TEM images confirmed the SEM results. The optical properties of the synthesized products were studied by UV–Vis spectroscopy and the results showed that by doping Fe^{3+} into the ZnO crystal lattice, the band gap is decreased and hence it can absorb more light than the bare ZnO. The photocatalytic activity of the product was examined by decomposition of methyl orange under ultraviolet radiation. The results showed that the product has high photocatalytic activity and it can decomposed dye structure by 62% that is mainly due to a decrease of the band gap of doped ZnO with respect to the bare ZnO one. The surface activity of the product was investigated by surface adsorption of the dye molecules on the nanostructure surface. The results showed due to high surface to volume ratio of the nanostructures, they could adsorb more than 65% of the dye and remove them from the solution. Another surface activity of the product was examined by removing Pb^{2+} from the water and the results were obtained by atomic absorption spectroscopy. The results showed that the product could remove Pb^{2+} more than 44% from the water.

✉ Mohammad Sabet
M.sabet@vru.ac.ir

[1] Department of Chemistry, Faculty of Science, Vali-e-Asr University of Rafsanjan, PO Box: 77176, Rafsanjan, Iran

1 Introduction

Zinc oxide (ZnO) is an optically transparent II–VI semiconductor and well-known piezoelectric and electro-optic material having hexagonal wurtzite structure with C^4_6v (P63mc) space group, wide direct band gap ($E_g = 3.37$ eV), exciton binding energy of 60 meV, and excellent mechanical characteristics [1]. ZnO nanostructures have a wide range of high technology applications like surface acoustic wave filters [2], photonic crystals [3], photodetectors [4], light emitting diodes [5], photodiodes [6], gas sensors [7], optical modulator waveguides [8], solar cells [9] and varistors [10]. Different nanostructures of ZnO have been reported such as nanowires and nanorods [11], nanocombs [12], nanorings [13], nanoloops and nanohelices [14], nanobows [15], nanobelts [16] and nanocages [17]. The presence of defects due to large surface to volume ratio of nanocrystals allows tuning various properties which can not be observed in their bulk form [18]. Doping semiconductor nanocrystals provide an additional means to control the optical, electrical and magnetic properties. For instance, band gap engineering is feasible [19] in transition metal ion-doped ZnO leading to different colors useful for optical devices [18]. Doping of semiconductors with transition metal elements, such as Mn, Fe, Co, etc., offers a viable means of tuning the optical band gap [20–22] as well as the ferromagnetic behavior [23–26]. Metal-doped ZnO is generally investigated in the form of diluted magnetic semiconductor (DMS) materials and a photocatalyst, because it shows much higher Curie temperature than room temperature, along with strong stability in UV light [27, 28]. In ZnO–Fe system general regularities are observed: with the growth of Fe dopant concentration the size of nanoparticles, crystallinity, and width of the bandgap zone decrease [29–34]. A visible - rays - active photocatalyst

is very important with respect to solar energy and interior lighting applications. For practical application, it has been reported that the enhancement of photocatalytic activity can be achieved by introducing foreign metal ions into ZnO or creating oxygen vacancies [35]. Until now, many scientists have been studying the methods to introduce foreign metal ions, such as W^{6+}, V^{5+}, and Fe^{3+}, etc., into ZnO. In particular, the Fe-doped case has been widely examined [36]. In this work, we synthesized different morphologies of Fe–ZnO nanostructures via a simple hydrothermal method. Different parameters were studied on the products size and morphology. The optical properties of the synthesized samples were investigated by UV–Vis spectroscopy. The photocatalytic activity of the product was investigated by decomposition of methyl orange as dye. Also, the surface activity of the nanostructure was studied by surface adsorption of dye molecules and lead ions from the aqueous medium.

2 Experimental

All the chemicals reagents used in the experiments such as $Zn(NO_3)_2.6H_2O$, $Fe(NO_3).9H_2O$, NaOH, CTAB, SDS and PEG were of analytical grade and used as received without further purification. XRD patterns were recorded by a Rigaku D-max C III, X-ray diffractometer using Ni-filtered Cu K_α radiation. Scanning electron microscopy (SEM) images were obtained on Philips XL-30ESEM equipped with an energy dispersive X-ray spectroscopy. UV–Vis spectra were recorded using a UV–Vis spectrophotometer (PerkinElmer). Transmission electron microscopy (TEM) images were obtained on zeiss transmission electron microscope. Fourier transform infrared (FT-IR) spectra were recorded on Shimadzu Varian 4300 spectrophotometer in KBr pellets. In a typical experimental procedure, 0.3 g of $Zn(NO_3)_2.6H_2O$ was dissolved in a certain amount of the distilled water. Another solution was prepared by dissolving a certain amount of $Fe(NO_3)_3.9H_2O$ (based on Table 1) in the distilled water under vigorous stirring. After that, two solutions were mixed together under stirring and pH of the final solution was adjusted to 12 with a NaOH solution. Then the reaction vessel was transferred to the autoclave and exposed to heating at different temperatures for different times. The obtained precipitates were collected and washed several times with distilled water and absolute ethanol and dried at 80 °C for 12 h. The experimental conditions are listed in Table 1.

3 Results and discussions

To study the crystallinity and crystallite size of the product, XRD analysis was used. For doped materials, XRD

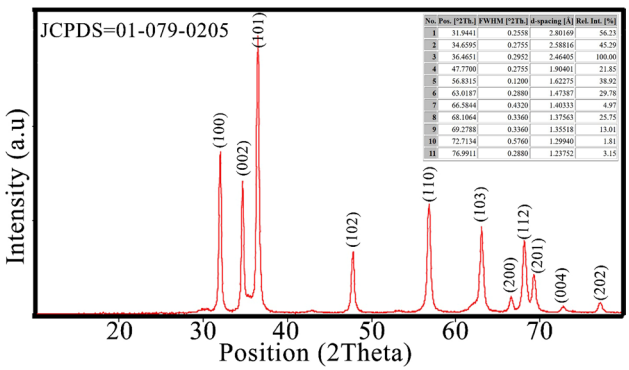

Fig. 1 XRD pattern of S9

Table 1 Sample preparation conditions

Sample no	$Zn(NO_3)_2.6H_2O$	$Fe(NO_3).9H_2O$	Surfactant	$Zn(acac)_2$	Temperature (°C)	Reaction time (h)
S1	0.3 g	0.03 g	SDS	–	180	24
S2	0.3 g	0.03 g	CTAB	–	180	24
S3	0.3 g	0.03 g	PEG	–	180	24
S4	0.3 g	0.03 g	–	–	140	24
S5	0.3 g	0.03 g	–	–	120	24
S6	0.3 g	0.03 g	–	–	180	18
S7	0.3 g	0.03 g	–	–	180	30
S8	–	0.03 g	–	0.3 g	180	24
S9	0.3 g	0.03 g	–	–	180	24
S10	0.3 g	0.02 g	–	–	180	24
S11	0.3 g	0.05 g	–	–	180	24

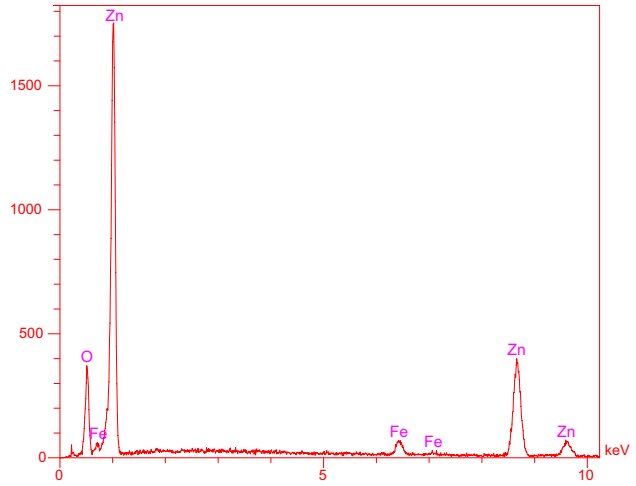

Fig. 2 EDS spectra of S9

can only show the formation of main phase and the presence of dopant must be investigated by EDS analysis. Figure 1 shows XRD pattern of the product. As shown in this figure the pattern is completely compatible with ZnO structure with hexagonal phase. It can be seen that the product is high pure and there are no peaks related to the other phases. The main peaks located at 32°, 35°, 36.5°, 47.8°, 56.9°, 63°, 66.2°, 68.3°, 69.2°, 73° and 77.3° are belonged to (100), (002), (101), (102), (110), (103), (200), (112), (201), (004) and (202) miller indices, respectively with JCPDS = 01-079-0205. EDS analysis was used to confirm doping ZnO nanostructure with Fe^{3+} (Fig. 2). It can be seen that the product is mainly composed of Zn, Fe and O elements. From the XRD result and EDS analysis, it can be concluded that ZnO was doped with Fe element. Also, the results showed that Fe^{3+} was inserted in the ZnO crystal lattice by 2.85 at.%. This doping amount can effect on the optical properties of the ZnO nanostructures. Figure 3 shows FT-IR spectra of the synthesized products. As shown in this figure all samples have similar spectra, which confirm that they have same structure. The peak at about 450 cm^{-1} is due to metal–oxygen bond. Also the peak at 1384 cm^{-1} is related to bending vibration of absorbed water molecules on the product surface. The broad peak located at 3400 cm^{-1} is related to the O–H stretching mode from the water adsorbed on the nanostructures surfaces. In fact, due to high surface of nanostructures they adsorb water molecules in the medium easily. Figure 4 shows SEM images of sample No. 9. It can be seen that the product is mainly composed of very tiny and aggregated particles. Also, beside the particles there are some

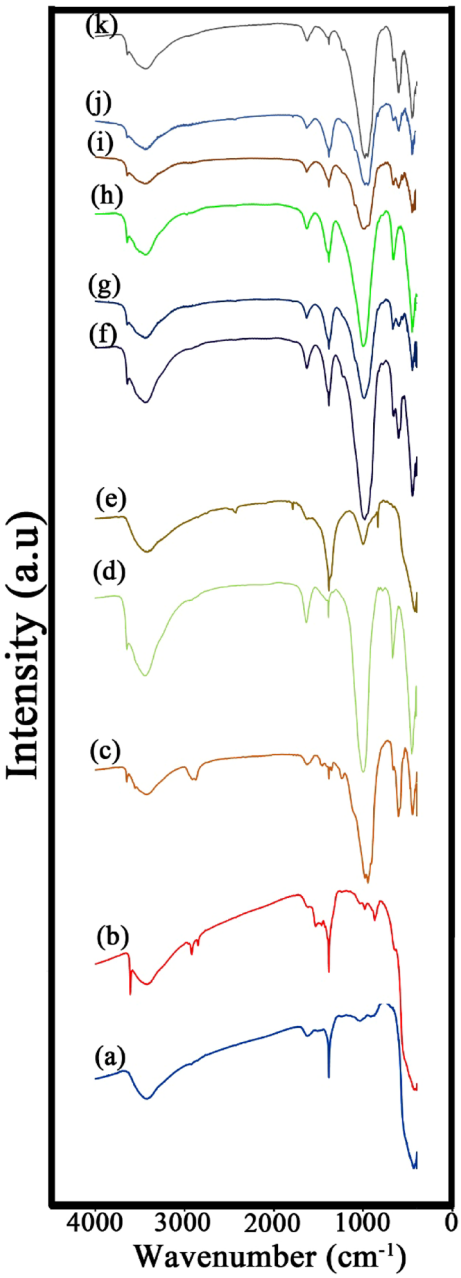

Fig. 3 *a–k* FT-IR spectra of the S1–S11, respectively

rod-like structures. In fact, in these conditions (180 °C and 24 h without surfactant), there are two different ways for nucleation and growth. Some nucleus created faster than the others create agglomeration structures. The others growth in one-dimensional and create large rod structures. In other words, without surfactant, the nucleation and growth were done in different ways and different morphologies can be observed in one product. To

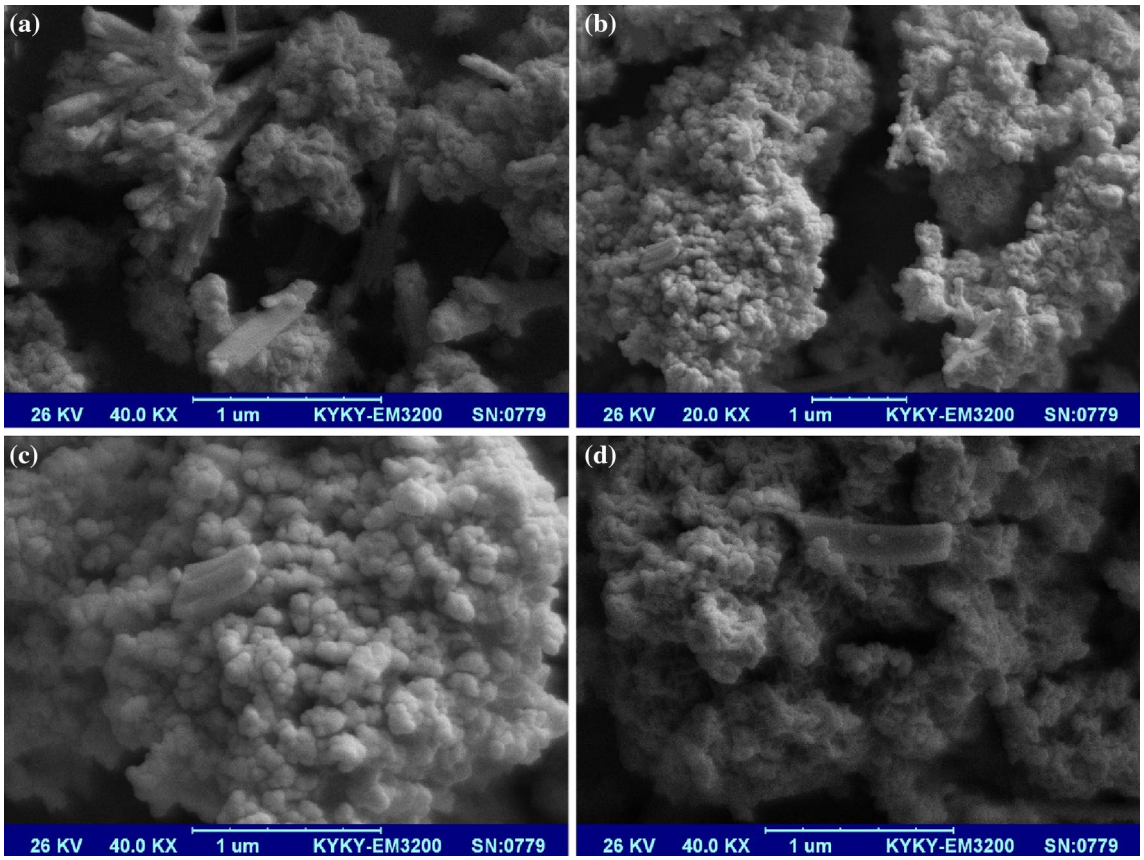

Fig. 4 **a–d** SEM images of S9

investigation of the surfactant effect on the product size and morphology, three different surfactants were used namely SDS as anionic surfactant, CTAB as cationic surfactant and PEG as neutral one. Figure 5a, b shows SEM image of sample No. (1) As shown in this figure, when SDS was used as surfactant very tiny and uniform nanoparticles were achieved. In fact, the SDS surfactant capped the created nucleus and prevent from agglomeration. SEM image of the product made from CTAB as surfactant is shown in Fig. 5c, d (sample No. 2). It can be observed that CTAB create the product with larger particles that is mainly due to higher steric hindrance of SDS respect to the CTAB. Another reason is related to net charge of the surfactant. ZnO has net positive charge under physiological conditions. Therefore, CTAB surfactant cant capped ZnO surface easily due to its positive charge and hence larger particles were obtained respect to the product created with negative SDS surfactant. Figure 5e, f shows SEM image of sample No. 3. It can be seen that the product is mainly composed of aggregated rod-like structures. In fact when PEG was used as neutral surfactant, it can only create steric hindrance around the nucleus surface and there are no any electrostatic repulsion among them. Therefore, the separation of nucleus from each other by PEG is weaker than SDS and CTAB and therefore the nucleus can join together and create some rod-like structures. Scheme 1 shows the effect of surfactant on the product size and morphology. To study the effect of reaction temperature on the product size and morphology, the reaction was done at three different temperatures (120, 140 and 180 °C). When the reaction was done at 120 °C, the product was mainly composed of small and aggregated particles (Fig. 6a, b). In fact in this temperature, the produced energy by the reaction medium is low and hence the nucleus have not enough energy to growth in specified direction. When the temperature was increased to 140 °C, the energy was increased and the growth was done at one direction and aggregated small

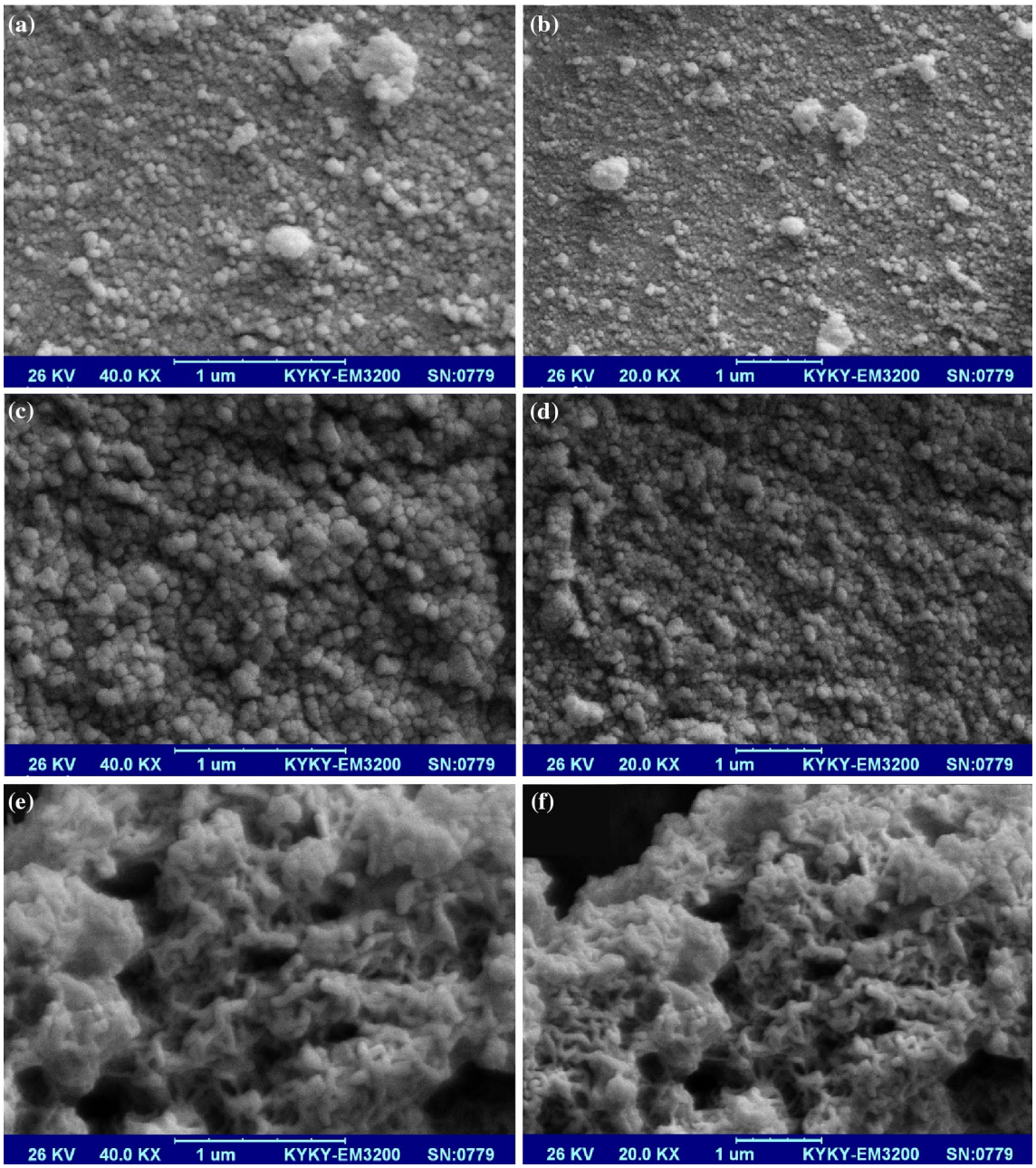

Fig. 5 SEM images of **a** and **b** S1, **c** and **d** S2 and **e** and **f** S3, respectively

rod-like structures were achieved (Fig. 6c, d). By further increase temperature (180 °C), the nucleus had enough energy to growth in specified direction and hence beside the small particles some rod-like structures were obtained (Fig. 4). So the temperature has significant effect on the product size and morphology and by increasing the temperature, the prepared energy is increased and hence the product morphologies are changed. Figure 7a, b shows SEM image of the product made at 180 °C for 18 h. It can be seen that the product is composed of some irregular shapes created from small rod structures. In fact, the reaction medium cannot create enough energy for produce small nanoparticles in this time. By increasing the time to 24 h, the product is composed of tiny nanoparticles and rod-like structures due to higher energy prepared in this time (Fig. 7c, d). By further increase of the

Scheme 1 Schematic of changing particle size and morphology by using different surfactant

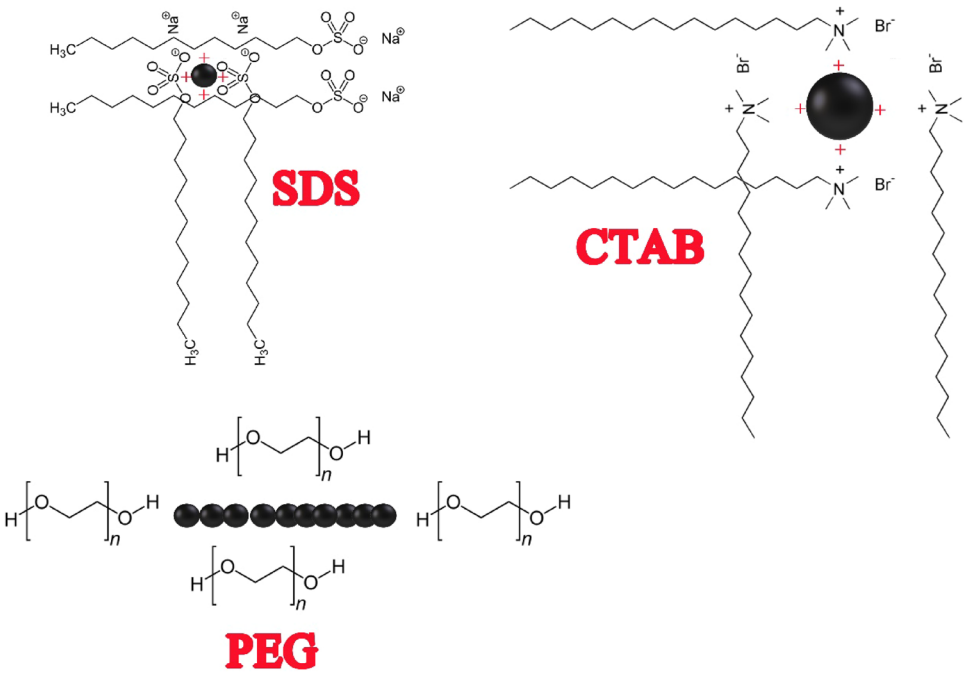

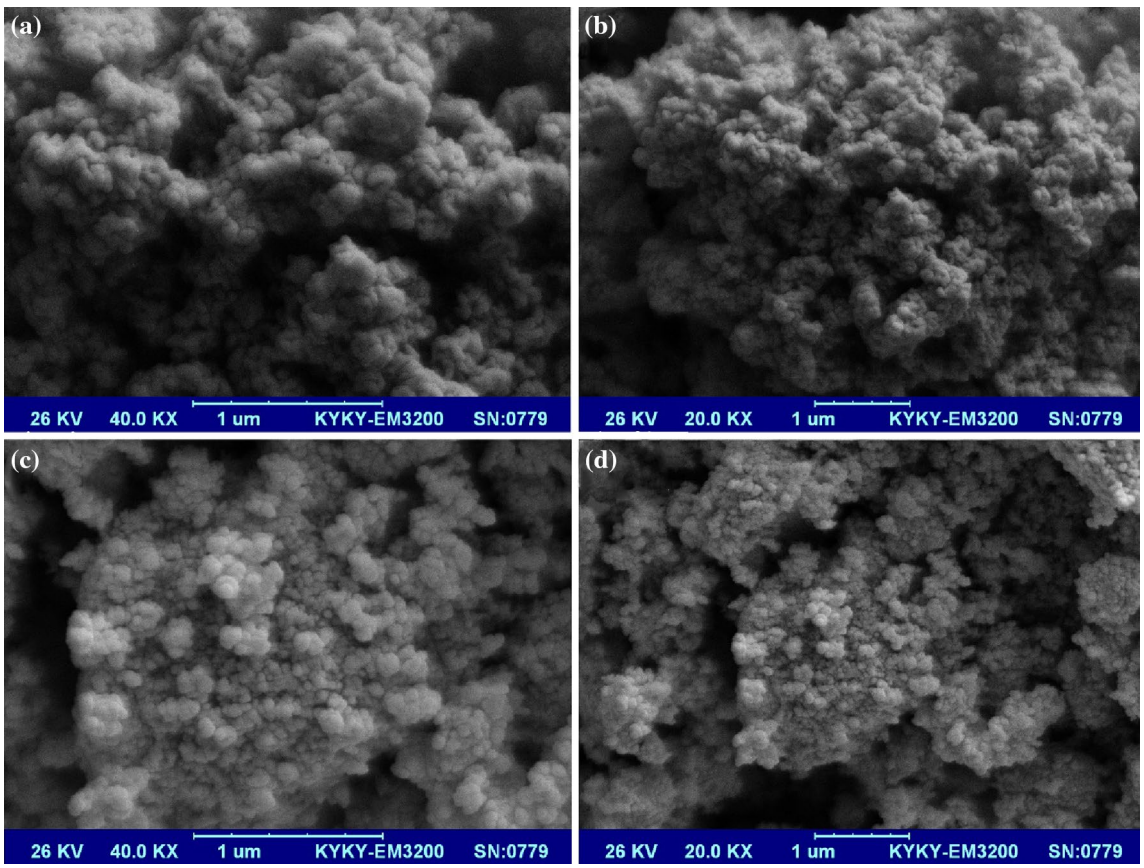

Fig. 6 SEM images of **a, b** S5 and **c, d** S4, respectively

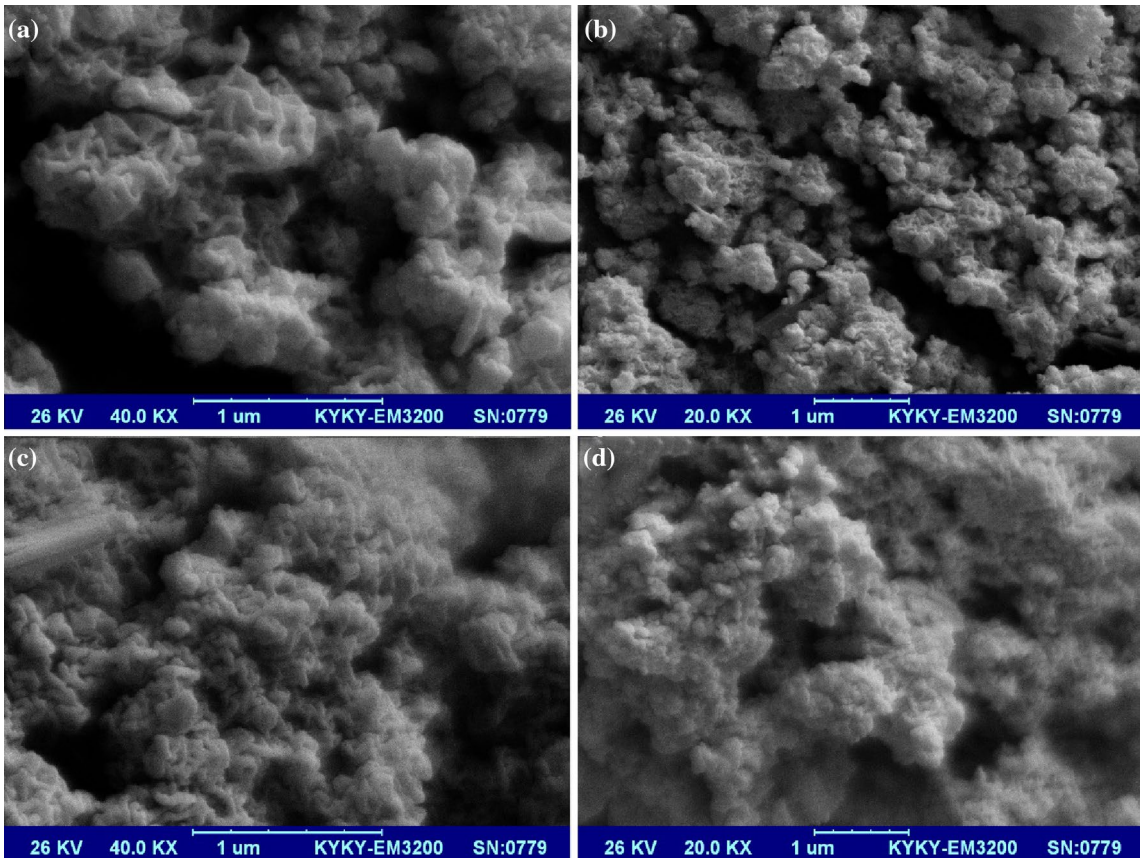

Fig. 7 SEM images of **a, b** S6 and **c, d** S7, respectively

reaction time, the energy prepared by the reaction medium was increased and due to high surface of nanoparticles, they aggregated together and large irregular shapes were created (Fig. 4). It can be concluded that the time plays important role in product size and morphology and by increasing it, the energy of the reaction medium is increased. The effect of Fe^{3+} percent in the ZnO structure on the product size and morphology was investigated by SEM image (Fig. 8). As shown in these figures, by increasing the Fe^{3+} percent in the ZnO structure, the uniformity of nanoparticles is increased. It can be said that by increasing the Fe^{3+} percent, the growth of ZnO nucleus is decreased and they have enough time to growth. Therefore, they can growth slowly and hence uniformity of the particles are increased. To investigate the steric effect on the product size and morphology, the ZnO–Fe nanostructures were synthesized via $Zn(acac)_2$ complex as precursor (Fig. 9). In fact, we used the complex to increase the steric hindrance. The result showed that the zinc complex creates small rod-like structures that is mainly due to higher steric hindrance around of the Zn^{2+} prepared with ligands. In other words, the ligands in the complex act like the surfactant and decrease the release rate of Zn^{2+}. Therefore, the nucleus have enough time to growth and hence smaller shapes are prepared. To further study about the product size and morphology, TEM analysis was used. Figure 10 shows TEM images of sample No. 9. As shown in these figures, the product is composed of nanorods and nanoparticle that is in agreement with SEM results. It can be seen that the product has uniform particles with about 60 nm diameter and it has nanorods created from aggregation of very tiny particles. To study the optical properties of the products, they were characterized by UV–Vis spectra. The results are shown in Fig. 11. As shown in this figure, all the products show higher absorption value than the bare ZnO nanostructure that is due to doping Fe^{3+} ions in the ZnO structure. In fact when Fe^{3+} is doped into the ZnO lattice structure, it decrease ZnO band gap. As shown in this figure each samples has different optical properties

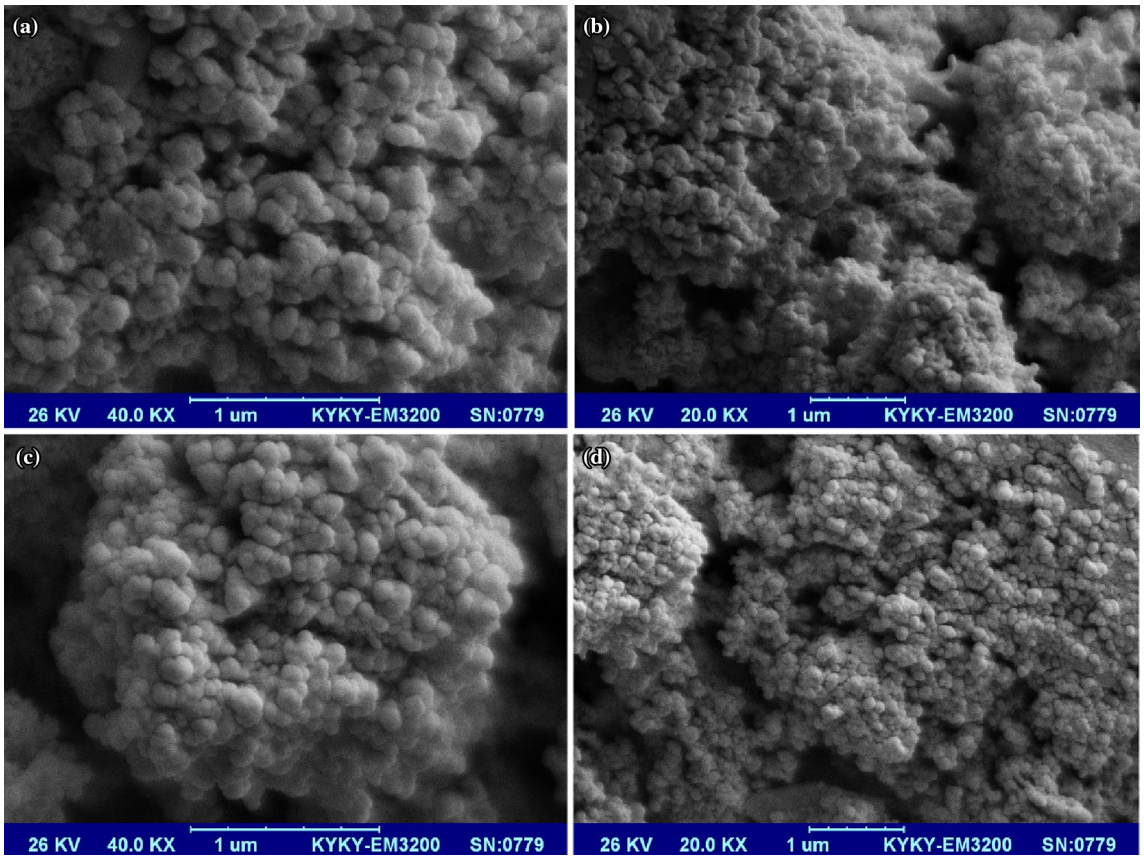

Fig. 8 SEM images of **a, b** S10 and **c, d** S11, respectively

that is mainly due to different particles size and morphologies of the prepared products. Indeed, by decreasing the particle size the band gap is increased and hence those products have larger particles show higher absorption values. Photocatalytic activity of the products were investigated by decomposition of methyl orange as dye. Figure 12 shows photocatalytic activity results. It can be seen that the photocatalytic activity of ZnO is increased by doping Fe^{3+} that is mainly due to decreasing ZnO band gap by Fe^{3+} doping. In fact, when Fe^{3+} decreases the ZnO band gap, it absorb more light and consequently more electrons are created to decompose the dye structure. Another reason for dye decompose is high surface of the nanostructures that can adsorb more dye molecules on their surfaces and hence catalysis the degradation of dye molecules. The mechanism of dye decomposition is shown in Scheme 2. In fact when the nanostructures are exposed to UV radiation, electron–hole pairs are created and the produced electrons decompose dye structure via a radical reaction. The surface activity of the product for dye adsorption was investigated. For this purpose, we dispersed ZnO–Fe powder to the dye solution and stirred for different times. After that, the solution was centrifuged and characterized with UV–Vis spectroscopy. As shown in Fig. 13 the prepared ZnO–Fe nanostructure has significant surface activity and they can adsorb dye molecules without any radiation. In fact, dye molecules can be adsorbed on the huge surface of the nanostructure and removed by a simple centrifuge process. Scheme 3 shows the schematic of surface dye adsorption. These results showed that the nanostructures could use as adsorbent to removing organic pollution from the water. To study the surface adsorption activity of the synthesized product, a solution of Pb^{2+} with certain concentration was prepared. After that, 0.1 g of the product was poured into the solution and stirred for 24 h. Then the solution was centrifuged and the remained Pb^{2+} was analyzed with atomic absorption spectroscopy (AAS). The results showed the

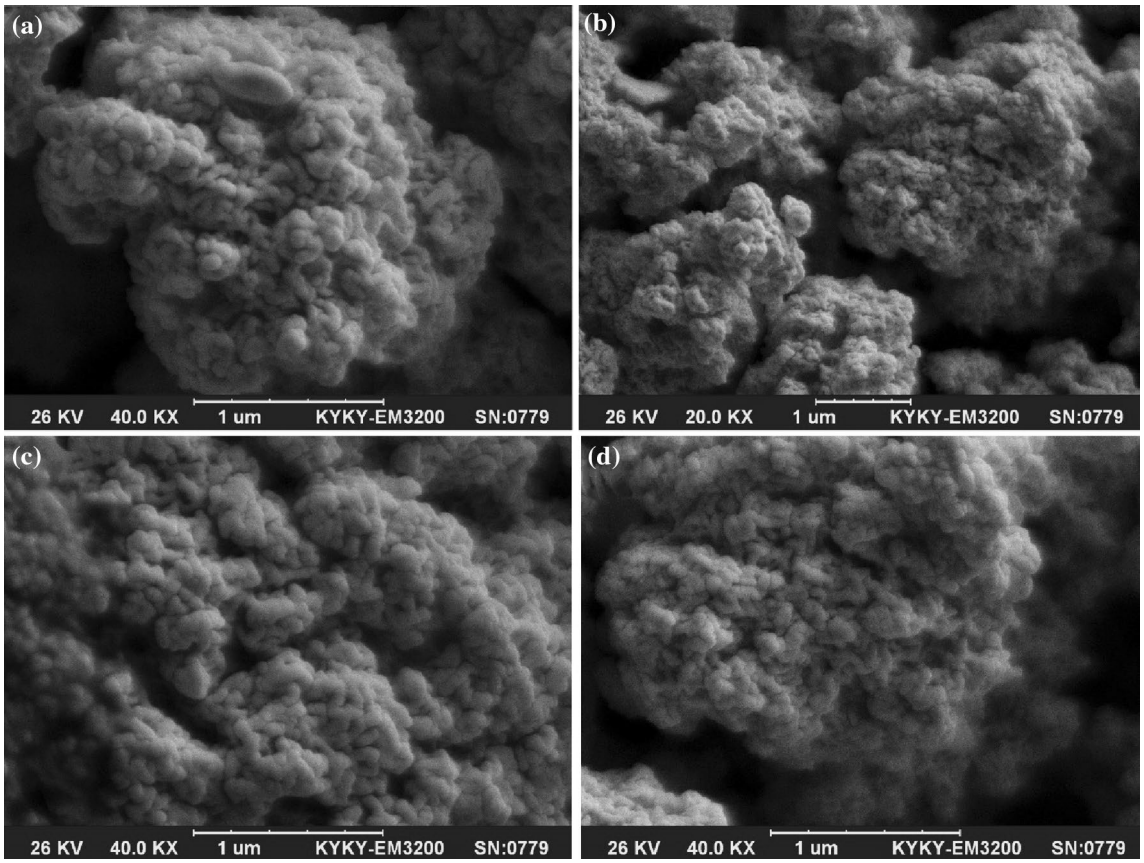

Fig. 9 **a–d** SEM images of S8

ZnO–Fe nanostructures adsorbed Pb^{2+} ions about 34% (Fig. 14). In fact, due to high surface to volume ratio of the synthesized nanostructures, they can adsorb Pb^{2+} from the aqueous medium and hence they are good candidate for water treatments applications.

4 Conclusion

In this work, different morphologies of Fe–ZnO nanostructures were synthesized via a simple hydrothermal method. Different parameters such as surfactant, reaction time and temperature, Fe source amount and Zn source kind were investigated on the product size and morphology. The results showed that by using different surfactants, different morphologies were obtained that is mainly due to different hindrance effects prepared with the surfactants. Also by changing the reaction time and temperatures, due to change of nucleation and growth rate, different morphologies were achieved. Another parameter that had significant effect on the product size and morphology was the amount of Fe^{3+} source. In fact, different Fe^{3+} sources change nucleation and growth rate and subsequently, the products take different morphologies. In addition, by using Zn complex as

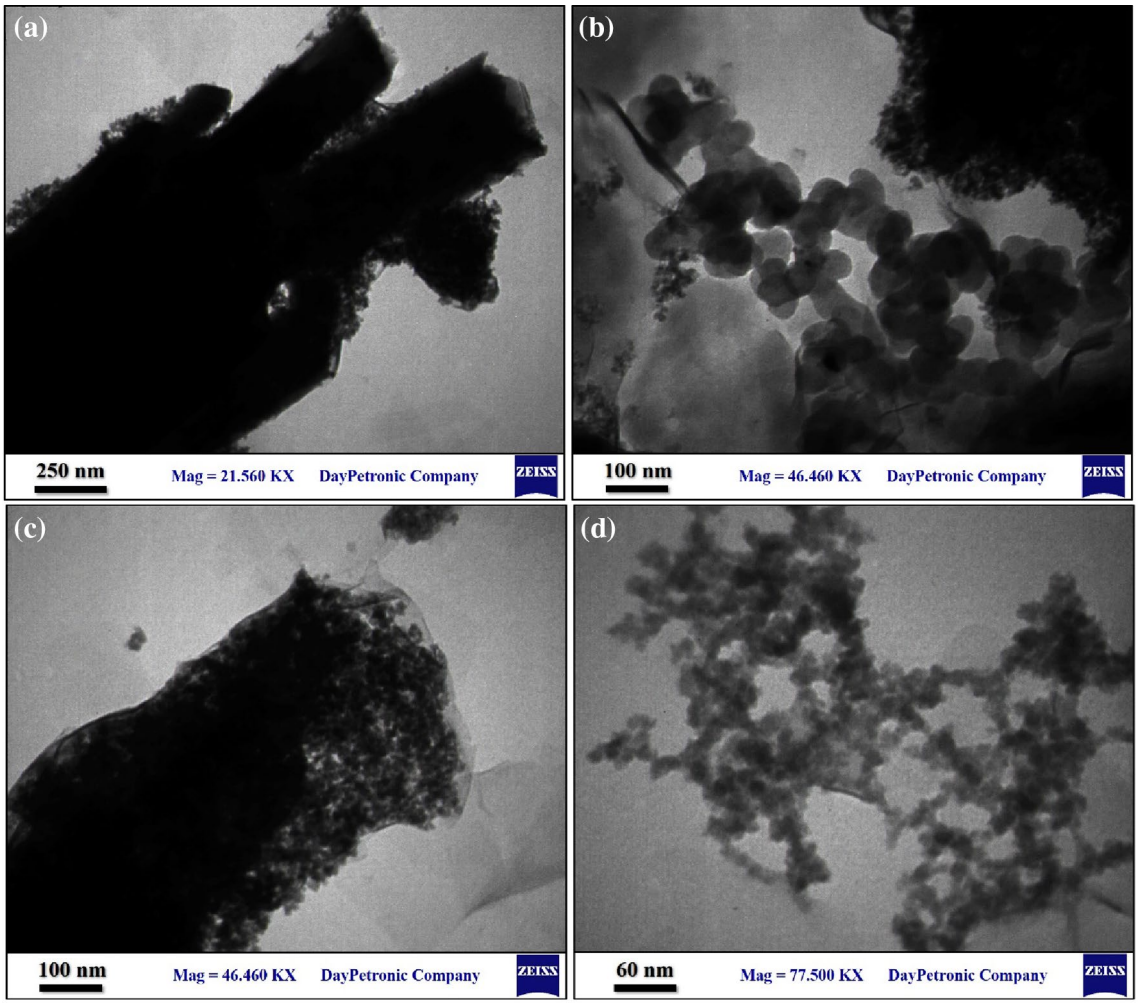

Fig. 10 **a–d** TEM images of S9

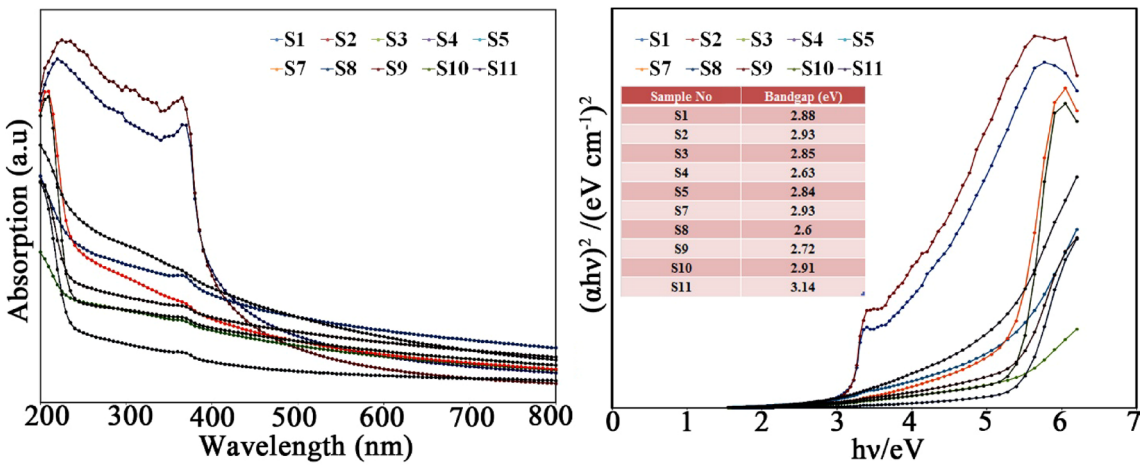

Fig. 11 UV–Vis spectra (*left*) and $(ahv)^2$ versus hv graphs (*right*) of the synthesized samples

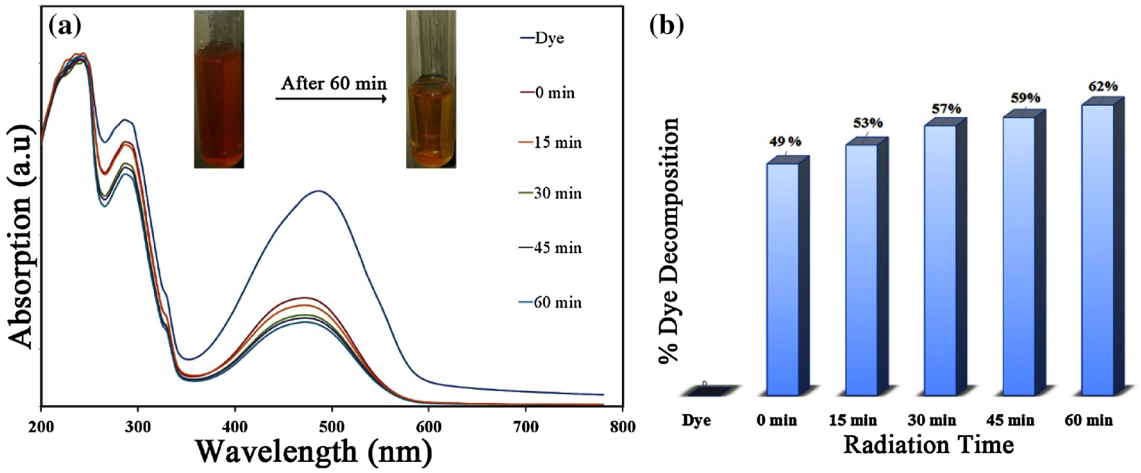

Fig. 12 **a** UV–Vis spectra of dye solution at different radiation times under S9 nanostructures presence and **b** % dye decomposition

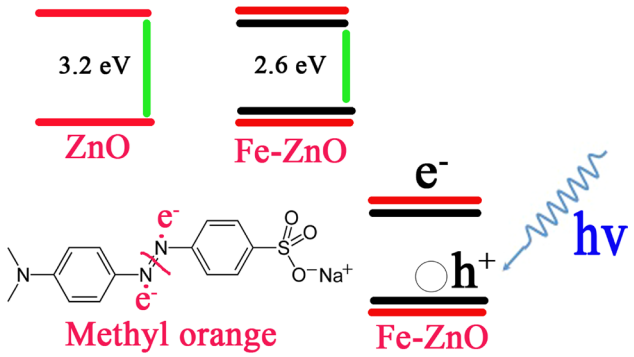

Scheme 2 Decreasing the ZnO band gap by doping Fe and degradation of methyl orange by Fe–ZnO nanostructures

precursor tiny structures were obtained that is due to steric hindrance prepared by the complex. The optical properties of the products were obtained by UV–Vis spectroscopy. The results showed each parameters has important effect on the optical properties and the band gaps of the products are changed in different orders. Investigation more about surface activity of the nanostructures was done by eliminating Pb^{2+} from the water via surface adsorption. The results showed the product remove Pb^{2+} from the water about 34% due to high surface to volume ratio of the product.

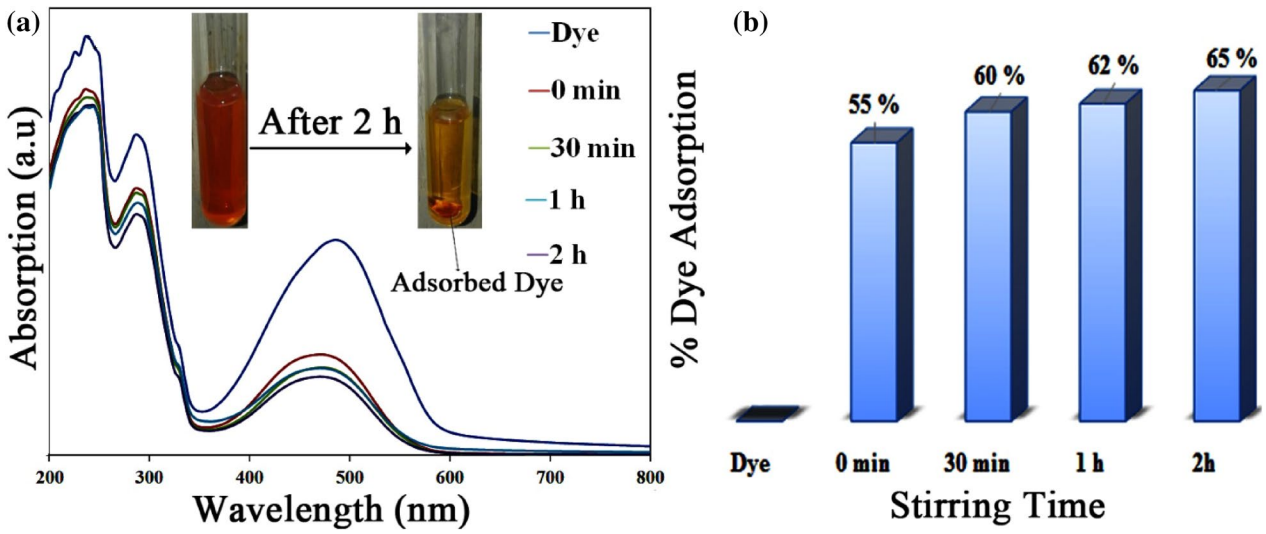

Fig. 13 **a** UV–Vis spectra of dye solution at different stirring times under S9 nanostructures presence and **b** % dye adsorption by the nanostructures

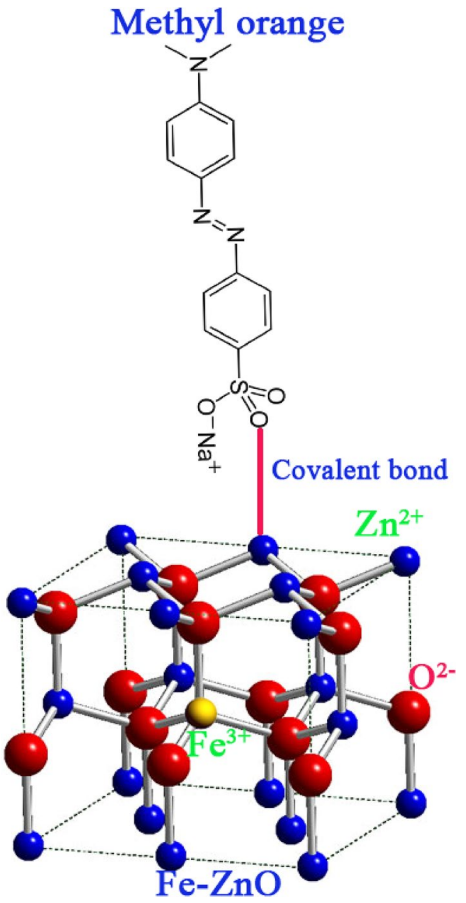

Scheme 3 Schematic of dye adsorption on the Fe–ZnO nanostructure

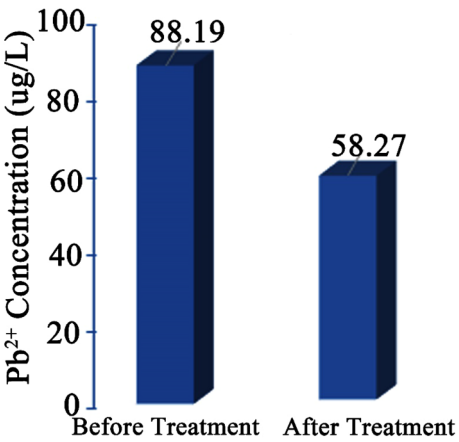

Fig. 14 Surface adsorption activity of the synthesized nanostructures

References

1. S. Kumar, K. Asokan, R.K. Singh, S. Chatterjee, D. Kanjilal, A.K. Ghosh, Structural and optical properties of ZnO and ZnO: Fe nanoparticles under dense electronic excitations. J. Appl. Phys. **114**, 164321 (2013)
2. N. Emanetoglu, C. Gorla, Y. Liu, S. Liang, Y. Lu, Epitaxial ZnO piezoelectric thin films for saw filters, Mater. Sci. Semicond. Process. **2**, 247–252 (1999)
3. Y. Chen, D. Bagnall, T. Yao, ZnO as a novel photonic material for the UV region, Mater. Sci. Eng. B **75**, 190–198 (2000)
4. S. Liang, H. Sheng, Y. Liu, Z. Huo, Y. Lu, H. Shen, ZnO Schottky ultraviolet photodetectors. J. Cryst. Growth **225**, 110–113 (2001)
5. N. Saito, H. Haneda, T. Sekiguchi, N. Ohashi, I. Sakaguchi, K. Koumoto, Low-temperature fabrication of light-emitting zinc oxide micropatterns using self-assembled monolayers. Adv. Mater. **14**, 418–421 (2002)
6. J. Lee, Y. Choi, J. Kim, M. Park, S. Im, Optimizing n-ZnO/p-Si heterojunctions for photodiode applications. Thin Solid Films **403**, 553–557 (2002)
7. P. Mitra, A.P. Chatterjee, H.S. Maiti, ZnO thin film sensor. Mater. Lett. **35**, 33–38 (1998)
8. M. Koch, P. Timbrell, R. Lamb, The influence of film crystallinity on the coupling efficiency of ZnO optical modulator waveguides. Semicond. Sci. Technol. **10**, 1523 (1995)
9. J.B. Baxter, A. Walker, K. Van Ommering, E. Aydil, Synthesis and characterization of ZnO nanowires and their integration into dye-sensitized solar cells. Nanotechnology **17**, S304 (2006)
10. Y. Lin, Z. Zhang, Z. Tang, F. Yuan, J. Li, Characterisation of ZnO-based varistors prepared from nanometre Precursor powders, Adv. Mater. Opt. Electron. **9** 205–209 (1999)
11. S. Baruah, C. Thanachayanont, J. Dutta, Growth of ZnO nanowires on nonwoven polyethylene fibers, Sci. Technol. Adv. Mater. **9**, 025009 (2008)
12. Y. Huang, Y. Zhang, X. Bai, J. He, J. Liu, X. Zhang, Bicrystalline zinc oxide nanocombs. J. Nanosci. Nanotechnol. **6**, 2566–2570 (2006)
13. W.L. Hughes, Z.L. Wang, Controlled synthesis and manipulation of ZnO nanorings and nanobows. Appl. Phys. Lett. **86**, 043106 (2005)
14. X.Y. Kong, Z.L. Wang, Spontaneous polarization-induced nanohelixes, nanosprings, and nanorings of piezoelectric nanobelts. Nano Lett. **3**, 1625–1631 (2003)
15. W.L. Hughes, Z.L. Wang, Formation of piezoelectric single-crystal nanorings and nanobows. J. Am. Chem. Soc. **126**, 6703–6709 (2004)
16. T. Sun, J. Qiu, C. Liang, Controllable fabrication and photocatalytic activity of ZnO nanobelt arrays. J. Phys. Chem. C **112**, 715–721 (2008)
17. M. Snure, A. Tiwari, Synthesis, characterization, and green luminescence in ZnO nanocages. J. Nanosci. Nanotechnol. **7**, 481–485 (2007)
18. D.Y. Inamdar, A.K. Pathak, I. Dubenko, N. Ali, S. Mahamuni, Room temperature ferromagnetism and photoluminescence of Fe doped ZnO nanocrystals. J. Phys. Chem. C **115**, 23671–23676 (2011)
19. Y. Wang, P.J. Thomas, P. O'Brien, Optical properties of ZnO nanocrystals doped with Cd, Mg, Mn, and Fe ions. J. Phys. Chem. B **110**, 21412–21415 (2006)
20. J. Sans, J. Sánchez-Royo, A. Segura, G. Tobias, E. Canadell, Chemical effects on the optical band-gap of heavily doped ZnO: M III (M = Al, Ga, In): an investigation by means of photoelectron spectroscopy, optical measurements under pressure, and band structure calculations. Phys. Rev. B **79**, 195105 (2009)
21. S. Kumar, S. Mukherjee, R.K. Singh, S. Chatterjee, A. Ghosh, Structural and optical properties of sol-gel derived nanocrystalline Fe-doped ZnO. J. Appl. Phys. **110**, 103508 (2011)

22. R. Krithiga, G. Chandrasekaran, Synthesis, strucutral and optical properties of vanadium doped zinc oxide nanograins. J. Cryst. Growth **311**, 4610–4614 (2009)
23. P.K. Sharma, R.K. Dutta, A.C. Pandey, Doping dependent room-temperature ferromagnetism and structural properties of dilute magnetic semiconductor ZnO: Cu^{2+} nanorods. J. Magn. Magn. Mater. **321**, 4001–4005 (2009)
24. J. Chaboy, R. Boada, C. Piquer, M. Laguna-Marco, M. García-Hernández, N. Carmona, J. Llopis, M. Ruíz-González, J. González-Calbet, J. Fernández, Evidence of intrinsic magnetism in capped ZnO nanoparticles, Phys. Rev. B **82**, 064411 (2010)
25. I. Balti, A. Mezni, A. Dakhlaoui-Omrani, P. Leone, B. Viana, O. Brinza, L.-S. Smiri, N. Jouini, Comparative study of Ni-and Co-substituted ZnO nanoparticles: synthesis, optical, and magnetic properties. J. Phys. Chem. C **115**, 15758–15766 (2011)
26. S. Pearton, C. Abernathy, M. Overberg, G. Thaler, D. Norton, N. Theodoropoulou, A. Hebard, Y. Park, F. Ren, J. Kim, Wide band gap ferromagnetic semiconductors and oxides. J. Appl. Phys. **93**, 1–13 (2003)
27. D.C. Look, Recent advances in ZnO materials and devices, Mater Sci. Eng. B **80**, 383–387 (2001)
28. X. Wu, Z. Wu, L. Guo, C. Liu, J. Liu, X. Li, H. Xu, Pressure-induced phase transformation in controlled shape ZnO nanorods. Solid State Commun. **135**, 780–784 (2005)
29. P. Dhiman, J. Chand, A. Kumar, R. Kotnala, K.M. Batoo, M. Singh, Synthesis and characterization of novel Fe@ ZnO nano-system. J. Alloys Compd. **578**, 235–241 (2013)
30. R. Saleh, N.F. Djaja, S.P. Prakoso, The correlation between magnetic and structural properties of nanocrystalline transition metal-doped ZnO particles prepared by the co-precipitation method. J. Alloys Compd. **546**, 48–56 (2013)
31. R. Saleh, S.P. Prakoso, A. Fishli, The influence of Fe doping on the structural, magnetic and optical properties of nanocrystalline ZnO particles. J. Magn. Magn. Mater. **324**, 665–670 (2012)
32. S. George, S. Pokhrel, T. Xia, B. Gilbert, Z. Ji, M. Schowalter, A. Rosenauer, R. Damoiseaux, K.A. Bradley, L. Mädler, Use of a rapid cytotoxicity screening approach to engineer a safer zinc oxide nanoparticle through iron doping. ACS Nano **4**, 15–29 (2009)
33. J. Anghel, A. Thurber, D.A. Tenne, C.B. Hanna, A. Punnoose, Correlation between saturation magnetization, bandgap, and lattice volume of transition metal (M = Cr, Mn, Fe, Co, or Ni) doped Zn1-xMxO nanoparticles. J. Appl. Phys. **107**, 09E314 (2010)
34. C. Xia, C. Hu, Y. Tian, B. Wan, J. Xu, X. He, Room-temperature ferromagnetic properties of Ni-doped ZnO rod arrays, Phys. E **42**, 2086–2090 (2010)
35. Y.R. Uhm, C.K. Rhee, C.S. Ju, Synthesis of Cu and Fe-doped ZnO nano-rod by hydrolysis of metal powders, Nanotechnology (IEEE-NANO), 2013 13th IEEE Conference on, IEEE, 2013, pp. 764–767
36. Q.A. Pankhurst, J. Connolly, S.K. Jones, J. Dobson, Applications of magnetic nanoparticles in biomedicine. J. Phys. D **36**, R167 (2003)